Materials Science and Engineering A 405 (2005) 313–320

www.elsevier.com/locate/msea

Thick ceramic thermal barrier coatings with high durability deposited using solution-precursor plasma spray

Amol Jadhav [a,1], Nitin P. Padture [a,*,1], Fang Wu [a], Eric H. Jordan [b], Maurice Gell [a]

[a] *Department of Materials Science and Engineering, Institute of Materials Science, University of Connecticut, Storrs, CT 06269-3136, USA*
[b] *Department of Mechanical Engineering, Institute of Materials Science, University of Connecticut, Storrs, CT 06269-3136, USA*

Received in revised form 3 June 2005; accepted 17 June 2005

Abstract

The efficacy of ceramic thermal barrier coatings (TBCs) used to protect and insulate metal components in engines increases with the thickness of the TBCs. However, the durabilities of thick TBCs deposited using conventional ceramics-coating deposition methods have not been adequate. Here, we demonstrate the feasibility of depositing highly durable, 4 mm thick TBCs of ZrO_2–7 wt.% Y_2O_3 (7YSZ) on bond-coated superalloy substrates using the solution-precursor plasma spray (SPPS) method. It was found that the average thermal cycling life of the 4 mm thick SPPS TBCs is 820 cycles. While most of the conventional air plasma-sprayed (APS) coatings of the same composition and thickness deposited on identical bond-coated superalloy substrates were found to be detached partially from the substrates in the as-sprayed condition, the APS TBC that was intact failed after 40 thermal cycles. The dramatic improvement in the thermal cycling life in the SPPS TBCs can be attributed to: (i) the significantly higher in-plane indentation-fracture toughness (over five-fold) in the SPPS TBCs over APS TBCs and (ii) the presence of the vertical cracks in SPPS TBCs resulting in a high degree of strain tolerance. The large thickness of the SPPS coatings also allowed us to characterize the mechanical properties of the ceramic top-coat in some detail. To that end, we report here the results from indentation-toughness tests and uniaxial-compression tests on the SPPS TBCs and the reference APS TBCs.

Keywords: Thermal barrier coatings; Plasma spray; Toughness; Compression; Thermal cycling

1. Introduction

Thermal barrier coatings (TBCs) made of low thermal-conductivity zirconia ceramics (ZrO_2–7 wt.% Y_2O_3 or 7YSZ) are routinely used to provide thermal insulation and protection to metallic turbine-engine components from the hot gas stream (see, e.g. reviews [1–3]). The use of TBCs (125–500 μm in thickness), along with internal cooling of the underlying metallic component, provides significant temperature reductions (100–200 °C) at the metal–ceramic interface. The air plasma spray (APS) process is used to deposit TBCs on metallic components in less critical areas within gas-turbine engines. The microstructure of APS TBCs is characterized by 15–25% porosity and large "splat" boundaries/cracks (~100 μm) that are parallel to the metal–ceramic interface. Although the "splat" boundaries/cracks result in reduced thermal conductivities in APS TBCs [4], they are the source of weakness in the TBCs and are responsible for the ultimate spallation failure of APS TBCs [5,6].

In this context, a new, potentially low-cost plasma spray deposition process was developed—solution-precursor plasma spray (SPPS) [7–9]—which offers the prospect of depositing highly durable TBCs that have low thermal conductivities. In the SPPS process, instead of the ceramic powder feedstock, which is used in conventional APS process, liquid-precursor solutions are injected directly into the plasma jet. Since the SPPS coatings deposition mechanisms are fundamentally different from those involved in the conventional APS process [10,11], SPPS coatings possess some unique microstructures that are highly desirable in TBCs [9,12,13].

* Corresponding author. Tel.: +1 614 247 8114; fax: +1 614 292 1537.
E-mail address: padture.1@osu.edu (N.P. Padture).
[1] Present address: Department of Materials Science and Engineering, Ohio State University, Columbus, OH 43210-1178, USA.

0921-5093/$ – see front matter © 2005 Elsevier B.V. All rights reserved.
doi:10.1016/j.msea.2005.06.023

A typical SPPS TBC is 300–500 μm in thickness, with the following key microstructural features [9–11]: (i) controlled porosity, (ii) through-thickness vertical cracks and (iii) a lack of large-scale "splat" boundaries that are omnipresent in APS TBCs. The porosity and the through-thickness cracks impart strain tolerance to the TBC, while the porosity also helps reduce the thermal conductivity. The lack of large-scale "splat" boundaries are thought to effectively toughen the ceramic, making SSPS TBCs highly durable relative to APS TBCs [9,12]. However, the mechanical properties of SPPS coatings have not been characterized in any detail.

While thin SPPS TBCs (300–500 μm) have shown great promise, the exceptional strain tolerance of SPPS coatings due to the presence of the through-thickness vertical cracks makes the SPPS process ideally suited for depositing thick TBCs (up to 4 mm thickness). This is in the context of a need for thick TBCs in gas-turbine engine, diesel engine and other applications, as thicker coatings are likely to result in unprecedented levels of temperature reductions across TBCs. Although conventional APS method has been used to deposit thick TBCs, either the durabilities of those TBCs have been inadequate or they require complex and expensive graded metal–ceramic interfaces [14,15].

In this study, we demonstrate, for the first time, the feasibility of depositing well-adherent 7YSZ TBCs of thickness ∼4 mm on bond-coated superalloy substrates using the SPPS method. We have also determined the thermal cycling durability performance of these ultra-thick TBCs. While the APS coatings of ∼4 mm thickness spalled either spontaneously or prematurely (40 cycles), the average thermal cycling durability of SPPS TBCs of the same thickness was found to be 820 cycles.

The large thickness of the SPPS coatings also allowed us to characterize the mechanical properties of the ceramic top-coat in some detail. To that end, we have characterized and compared the indentation-toughness and uniaxial-compression properties of the SPPS TBCs, along with the reference APS TBCs.

2. Experimental

2.1. Coatings preparation

The SPPS and APS coatings were deposited using the direct current (dc) 9 MB plasma torch (Sulzer Metco, Westbury, NY), which was attached to a six-axis robotic arm. A set of APS and SPPS coatings were deposited on the grit-blasted, plasma-preheated (preheating temperature ∼ 200 °C) 304 stainless steel coupons, which were either disks (diameter 25.4 mm, thickness 4 mm) or plates (50 mm × 70 mm × 4 mm). Another set of APS and SPPS coatings were deposited on bond-coated superalloy substrates (disks: diameter 25.4 mm, thickness 4 mm) obtained from a commercial source. Only one surface (circular or rectangular) of each specimen was coated. For SPPS coatings, the feedstock used was an aqueous precursor solution of zirconium and yttrium salts, to result in a solid solution of 93 wt.% ZrO_2 and 7 wt.% Y_2O_3 (7YSZ) in the coating (Inframat Corp., Farmington, CT). The APS coatings of similar composition were deposited using a powder feedstock (Metco 204N, Sulzer Metco, Westbury, NY). Coatings of thicknesses 3.4 or 4 mm were obtained using both the methods. Most of the APS coatings were found to be detached partially from the substrates during deposition.

In order to obtain fully free-standing coatings, the as-sprayed SPPS and APS specimens (stainless steel substrates only) were dipped in a 40% HNO_3 solution for 2 h, where the acid attacked selectively the partially attached metal–ceramic interfaces. The free-standing coatings were cleaned thoroughly and dried before further preparation.

The densities of the free-standing SPPS and APS coatings were measured using the Archimedes principle, with deionized water as the immersion medium.

In order to study the effects of heat-treatment on the mechanical properties, some of the free-standing SPPS coatings were heat-treated at 1100 °C for 2 h in air using a box furnace (Thermolyne, Dubuque, IA).

2.2. Fracture toughness measurements

Cross-sections of the SPPS and the APS coatings were polished to a 1 μm finish using routine ceramics polishing techniques. These polished cross-sections were indented using Vickers diamond pyramid with a contact load (P) of 49 N (five indentations per material). Care was taken to align the diagonals of the square Vickers impression as shown in Fig. 1A. Radial cracks, emanating from the indentation corners, running parallel to the deposition surface are referred to as "in-plane," while those perpendicular to that surface are referred to as "out-of-plane." The sizes of the hardness impressions (a) and sizes of the in-plane and out-of-plane cracks (c) were measured using a scanning electron microscope (SEM) (ESEM 2020, Philips Electron Optics, The Netherlands). The hardness (H) was determined using the equation: $H = P/2a^2$ [16]. The formulation due to Lawn [16] was used to determine the in-plane and the out-of-plane toughness values: $K_{IC} = 0.016(E/H)^{0.5}Pc^{-1.5}$. The elas-

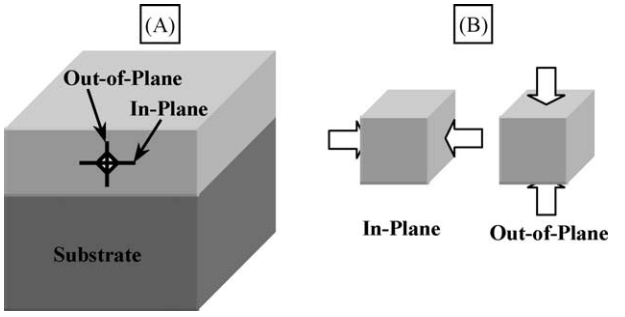

Fig. 1. Schematic illustration showing in-plane and out-of-plane orientations for: (A) indentation test and (B) uniaxial-compression test.

tic modulus (E) was measured using uniaxial-compression testing.

2.3. Compression testing

The free-standing SPPS and APS coatings were carefully diced into cubes (3.3 mm^3) using a precision saw (Isomet 1000, Buehler, Lake Bluff, IL) equipped with diamond wafering blade and all surfaces were polished to a 1 μm finish. The cube specimens were then tested in uniaxial compression using a screw-driven mechanical testing machine (Model 5869, Instron Corp., Canton, MA) in two different orientations—in-plane and out-of-plane—as shown schematically in Fig. 1B. For compression testing, the cube specimen were sandwiched between two highly polished tungsten carbide platens. Full articulation of the platens and appropriate positioning fixtures assured alignment of the specimens with the loading axis. The load was measured using a calibrated load cell and the platen displacement was measured using precision extensometers mounted between the platens. The contact between the specimen and the platens was lubricated with grease. The specimens were tested either in load control (20 N s^{-1}) mode or displacement control (0.001 mm s^{-1}) mode.

Two types of uniaxial-compression tests were conducted. In the first type of test, the specimens were loaded in displacement control until failure occurred. This test allowed us to evaluate the compressive elastic moduli and the average ultimate compression strengths of the SPPS and the APS coatings. At least four specimens were tested per materials and orientation. In the second type of test, the specimens were loaded in load control up to a peak load of 300 N and they were fully unloaded, which constituted the first cycle. The same specimens were then subjected to a second cycle and a third cycle where the peak loads were 600 and 1000 N, respectively. The latter tests allowed us to study the mechanical hysteresis in the SPPS and the APS coatings.

2.4. Thermal cycling

Thermal cycling testing of the 4 mm thick APS and SPPS TBCs on bond-coated superalloy substrates was carried out using an automated thermal cycling furnace (CM Inc., Bloomfield, NJ). The thermal cycle consisted of a 5 min heat-up from room temperature to 1121 °C, a 45 min hold at that temperature, followed by a 10 min forced-air quench to room temperature. A sample was considered to have failed when the area fraction of the detached TBC from the substrate reached ∼0.5. A total of four SPPS TBC specimens were tested. Only one reference 4 mm thickness APS TBC specimen could be tested because most APS coatings were found to be partially detached from the substrate during deposition. Partial detachment of thick APS TBCs during deposition has been observed by others (see, e.g. [17]).

3. Results and discussion

3.1. Microstructures

Fig. 2A shows cross-sectional SEM micrographs of a thick SPPS coating at low and high magnifications, respectively. These thick SPPS coatings are characterized by branched vertical cracks, this is in contrast with thin SPPS coatings (250–300 μm), where unbranched vertical cracks are observed [9–11]. The vertical cracks are a representation of separated columns running perpendicular to the substrate/coating interface. The separated vertical columns appear as “mudflat” pattern from the top, as seen in the top-view optical micrograph in Fig. 3. As the coating becomes thicker, columns with larger diameters become more stable, which manifests itself as branched vertical cracks in the cross-section view.

The higher magnification SEM micrograph of SPPS coating cross-section (Fig. 2A) shows a lack of horizontal “splat” boundaries/cracks. Such horizontal “splat” boundaries/cracks are always present in APS coatings, as seen in the cross-sectional SEM micrograph of the free-standing APS coating (Fig. 2C) and they can be up to 100 μm long. Long vertical cracks were not present in the APS coatings.

The densities of the SPPS and the APS coatings were determined to be 4.73 and 5.16 Mg m^{-3}, respectively. Assuming that fully dense 7YSZ has a density of 6.07 Mg m^{-3}, the porosity in the SPPS coating is ∼22% and that in APS coating is ∼15%. It is important to note that the porosity of the SPPS coatings can be tailored between 5 and 40% by adjusting the processing conditions. Fig. 2B shows that the porosity in the SPPS coating is isotropic and randomly distributed. In contrast, the pores in the APS coating (Fig. 2C) are sheet-like and aligned along the substrate/coating interface.

The microstructures of APS ceramic coatings have been studied extensively and the mechanisms by which they arise have been documented in the literature [18,19]. In the case of SPPS coatings, an understanding of their deposition mechanisms is beginning to emerge [9–11,20]. It has been shown that the SPPS coatings form by fundamentally different mechanisms relative to APS coatings, which result in the isotropic porosity and the lack of “splat” boundaries/cracks in the SPPS coatings. It has also been shown that the formation of the vertical cracks in SPPS coatings is due to a combined effect of thermal-expansion-mismatch stresses and stresses arising from the pyrolysis of remnant precursor embedded within the coating during the deposition process [21].

3.2. Hardness and fracture toughness

Fig. 4A and B shows SEM micrographs of Vickers indentation sites in SPPS and APS coatings, respectively. At the same magnification, the hardness impression in the SPPS coating is seen to be smaller than the one in the APS coating. The average hardness values of the SPPS and the APS

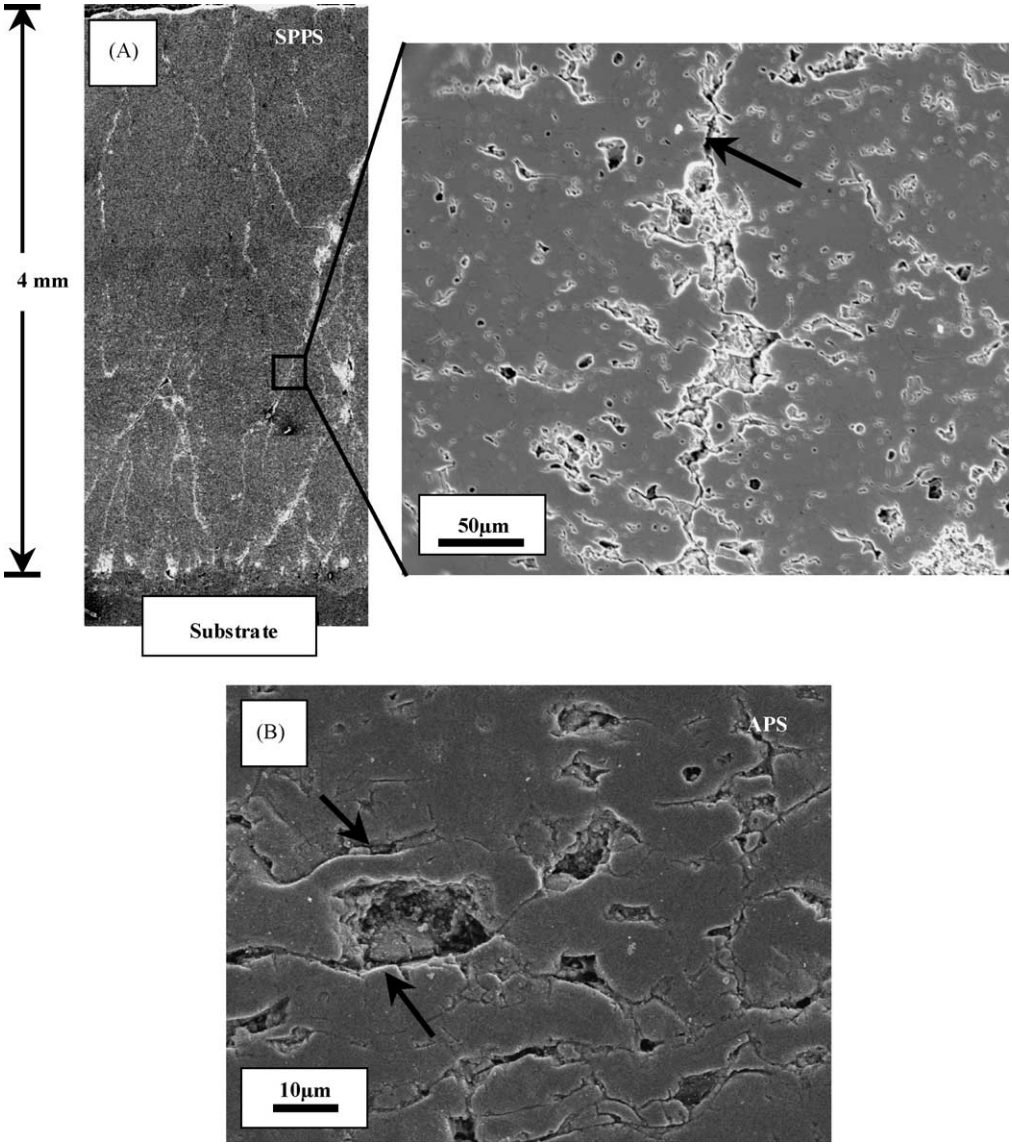

Fig. 2. (A) Cross-sectional SEM micrograph of a SPPS coating at low and high magnifications. Arrow indicates a vertical crack in the high-magnification micrograph. (B) Cross-sectional SEM micrograph of APS coating showing "splat" boundaries (arrows).

coatings were determined to be 5.4 GPa (range 6.2–4.1 GPa) and 3.9 GPa (range 4–3.6 GPa), respectively. It is not clear why the hardness of the SPPS coatings is higher than that of the APS coating, despite the higher porosity in the SPPS coatings.

The in-plane crack in the SPPS coatings (Fig. 4A) appears to be significantly shorter than that in the APS coating (Fig. 4B). The in-plane crack in the APS coating appears to follow the "splat" boundaries (Fig. 4C). This behavior is similar to what has been observed in other studies on crack-propagation in APS coatings using micro-mechanical testing devices (not indentation) [22]. The in-plane elastic moduli for SPPS and APS coatings estimated from the compression tests (Section 3.3) were used in calculating the indentation-toughness values reported in Fig. 5. It can be seen clearly that the in-plane indentation toughness of SPPS coating is over five times that of APS coating. This is particularly important because the plane parallel to the metal–ceramic interface (in-plane) within the ceramic top-coat is the primary location of spallation failure in plasma-sprayed TBCs [5,6]. The lower in-plane toughness in the APS coatings can be attributed to the presence of weak, long "splat" boundaries and cracks in that orientation. Although "splat" boundaries exist in SPPS coatings, they are 50–100 times smaller than those found in APS coatings [11]. This is due to the fundamentally different deposition mechanisms in SPPS that result in "ultra-fine splats" that are 1–5 μm in diameter compared to the "splats" in APS coatings that are ∼100 μm in diameter [11].

The in-plane and the out-of-plane cracks in the SPPS coating appear to be similar in length in Fig. 4A. Thus, the toughness of the SPPS coating is isotropic within 30% (Fig. 5). This is expected considering the random nature of the SPPS

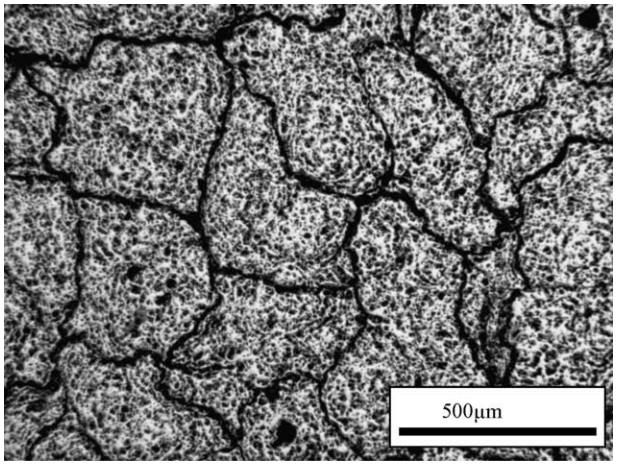

Fig. 3. Top-view optical micrograph of a SPPS coating showing the "mud-flat" pattern.

coating microstructure. In the case of the APS coatings, well-defined out-of-plane cracks could not be found, precluding estimation of the indentation-toughness APS in the out-of-plane orientation. Out-of-plane cracks in APS are likely to

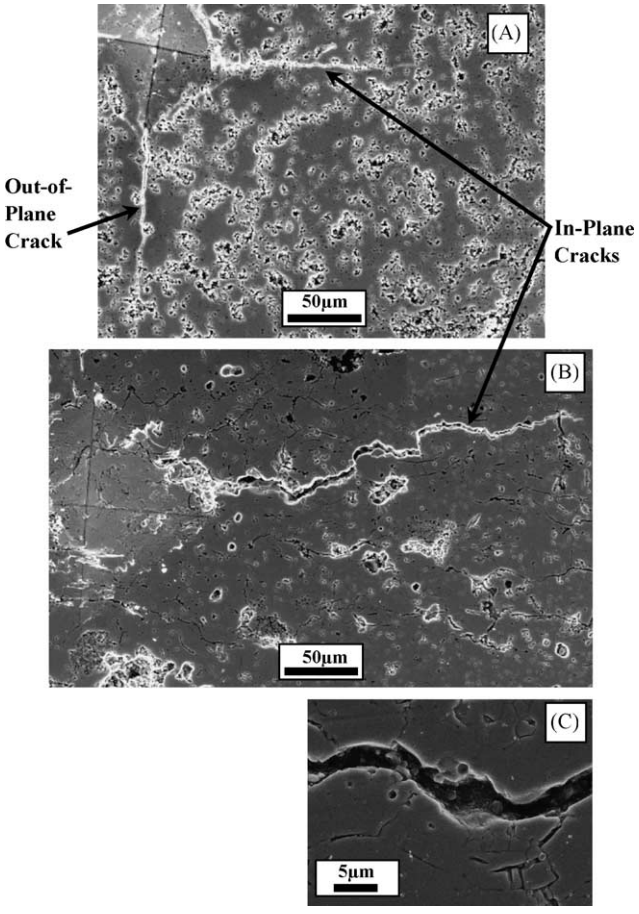

Fig. 4. SEM micrographs of Vickers indentation (49 N load) sites in: (A) SPPS coating and (B) APS coating. Arrows indicate in-plane and out-of-plane cracks. (C) High-magnification SEM micrograph showing the in-plane indentation crack following a "splat" boundary in the APS coating.

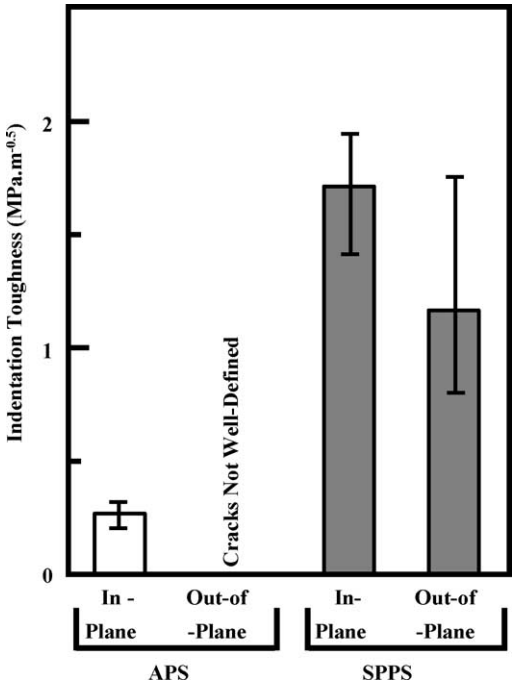

Fig. 5. Indentation toughness of the SPPS and APS coatings. The histogram represents the average readings from five indentations and the error bars represent the data range. The toughness in the out-of-plane orientation in the APS coating could not be estimated because well-defined cracks did not form in that coating.

be heavily bridged by the "splats" that run perpendicular to the cracks, resulting in crack arrest. Thus, the highly textured microstructures in APS coatings result in the extremely pronounced toughness anisotropy. Such anisotropy in the indentation toughness of APS ceramic coatings has been reported by others (see, e.g. [23,24]).

In a recent study, Choi et al. [25] measured the toughness, using conventional methods (single-edge V-notch beam (SEVNB) and double cantilever beam (DCB)), of free-standing 8YSZ APS coatings in the in-plane and out-of-plane orientations. They found the toughness to be isotropic. This apparent discrepancy can be explained based on the rising *R*-curve behavior—initial increase in toughness with crack length followed by a toughness plateau [16]—observed in APS TBCs due to crack-bridging [22]. Generally, the indentation-test samples the short-crack region of the *R*-curve, while the conventional toughness tests (DCB) sample the long-crack plateau region [16]. Due to the heterogeneous nature of the APS coatings, it appears that the *R*-curve for the cracks in the in-plane orientation rises slowly with the crack size, resulting in a low toughness value in the indentation test but a high plateau toughness. In contrast, the *R*-curve in the out-of-plane orientation is expected to rise steeply with crack size due to crack-bridging by "splats", making it difficult to measure the short-crack toughness using indentation. Since micro-mechanisms of APS TBC failure are largely controlled by local, or short-crack, toughness [5,6], the in-plane indentation toughness is the most relevant toughness in the

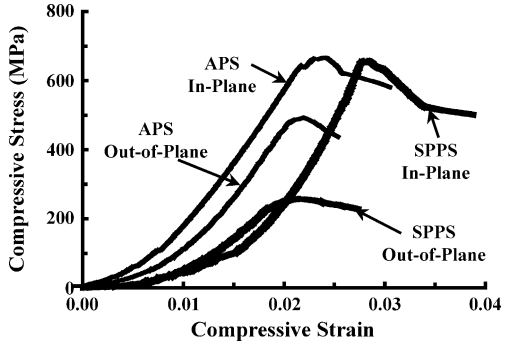

Fig. 6. Typical uniaxial-compression stress–strain curves for SPPS and APS coatings in in-plane and out-of-plane orientations.

context of TBC failure. Although the ultimate spallation failure of APS TBCs is a long-crack phenomenon, it is the result of a complex link-up of multiple short-cracks [5,6], which is quite different from the propagation of single, dominant long-cracks used in conventional toughness tests.

3.3. Compression behavior

Fig. 6 shows typical compression stress–strain responses of SPPS and APS coatings tested in in-plane and out-of-plane orientations. The in-plane stress–strain curves for both materials are characterized by non-linear deformation behavior, followed by linear behavior prior to failure. The hysteresis observed in the stress–strain behavior at low stresses (Fig. 7A and B; Table 2) further confirms the permanent deformation in the SPPS and the APS coatings during uniaxial compression. The hysteresis in both coatings is characterized by an increase in the secant elastic modulus with successive load–unload cycles (Table 2). The non-linear compression (uniaxial) behavior in APS coatings has been observed by others [25–28] and it has been attributed to the sliding of microcracks in the coating. With increasing compressive stress, microcracks close-up, resulting in elasticity, characterized by a linear stress–strain response. This is followed by the failure of the coating. In the case of the SPPS coating, the non-linear response can be attributed to cracking and sliding at the pores, followed by compaction; this has been observed by others in porous ceramics [29,30]. The more pronounced deformation (strain) in the SPPS coating could be due to the higher porosity in the SPPS coating compared to the APS coating.

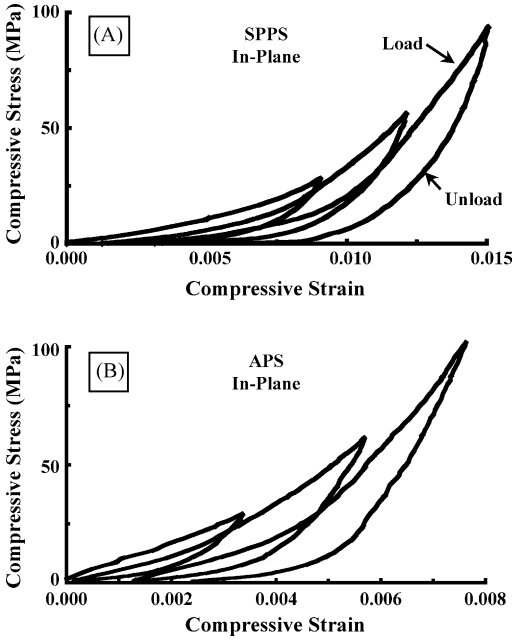

Fig. 7. Typical uniaxial-compression stress–strain curves during three cycles of loading–unloading with successively increasing loads: (A) SPPS coating and (B) APS coating. The loading and unloading parts of the curves are marked in (A).

Table 1
Elastic modulus and compressive strength of SPPS and APS coatings

Coating	Orientation	Average elastic modulus (range) (GPa)	Average compression strength (range) (MPa)
SPPS	In-plane	49 (77–44)	540 (722–301)
	Out-of-plane	22 (30–9)	258 (306–190)
SPPS (heat-treated)	In-plane	100 (122–71)	629 (697–504)
	Out-of-plane	67 (75–58)	368 (424–306)
APS	In-plane	40 (47–35)	578 (648–423)
	Out-of-plane	38 (41–32)	476 (591–335)

The in-plane ultimate compressive strengths and the elastic moduli for SPPS and APS coatings are reported in Table 1. The linear portions of the stress–strain curves were used to estimate the elastic moduli. The compressive strengths and the elastic moduli for the two coatings are observed to be comparable. This is probably because the high-stress behavior is dominated by the compacted material in both cases, where the microstructural differences are less likely to have an effect. The difference in the microstructures is manifested in the low-stress behavior, where more pronounced deformation is observed in the SPPS coating.

The compression stress–strain behavior for APS coatings in the two orientations is quite similar, with the ultimate compressive strength in the out-of-plane orientation being

Table 2
Maximum stress and elastic modulus for repeated compressive loading–unloading of SPPS and APS coatings

Coating/orientation	Cycle number	Maximum stress (MPa)	Secant modulus (GPa)
SPPS/in-plane	1	27	3.1
	2	55	7.7
	3	93	13.6
APS/in-plane	1	32	10.3
	2	68	13.4
	3	110	17.3

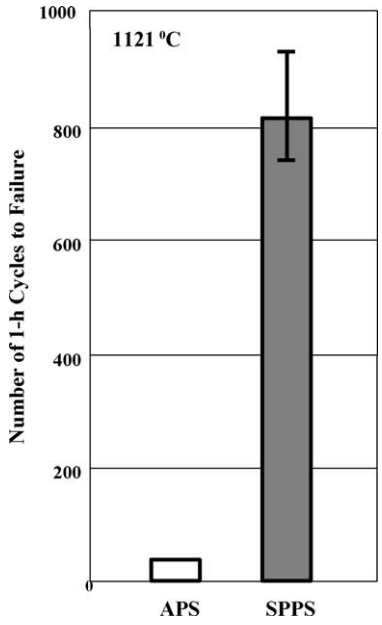

Fig. 8. Thermal cycling durability of APS and SPPS ultra-thick TBCs (∼4 mm thickness) on bond-coated superalloy substrates. Only one APS TBC specimen could be tested. The SPPS histogram represents the average of four specimens and the error bars represent the data range.

somewhat lower. In contrast, the SPPS coating is significantly more compliant and weaker in the out-of-plane orientation. This can be attributed to the vertical cracks in the SPPS coatings, which are likely to dominate the compression behavior at the macro-scale—easy sliding and failure is likely to occur along these vertical cracks in the out-of-plane orientation.

Since the Vickers indentation-toughness test involves large local deformations at the microstructural level, the in-plane elastic modulus is considered to be the most relevant in the toughness calculations [31].

Upon heat-treatment, the SPPS coatings become stiffer and stronger in both the in-plane and out-of-plane orientations (Table 1). This is most likely due to the heat-treatment-induced complete pyrolysis of the unpyrolyzed material that is ubiquitously present in the as-sprayed SPPS coatings [11].

3.4. Thermal cycling

Fig. 8 shows the relative thermal cycling lives of APS and SPPS TBCs. The dramatically improved durability in the SPPS TBCs is clearly evident from these results. This improved durability can be attributed to the two unique features of the SPPS TBCs. First, the local fracture toughness of the SPPS coating is over five times that of the APS coating in the in-plane orientation, the plane in which spallation failure of APS TBCs occurs [5,6]. As the driving force for the spallation failure of the TBC increases with the number of thermal cycles [5,6], an increased in-plane fracture toughness is bound to contribute to the delay in the spallation failure of SPPS TBCs. Second, the vertical cracks in the SPPS TBCs contribute significantly to the strain tolerance of the TBCs [9,32], thereby, reducing the rate of stress build-up within the coating that leads to spallation. Detailed failure mechanisms and analysis of thick SPPS TBCs will be the subject of a separate publication.

4. Summary

The SPPS method has been used to demonstrate the feasibility of depositing highly durable, thick (4 mm thickness) 7YSZ TBCs on bond-coated superalloy substrates. The microstructures of these coatings are characterized by vertical cracks, a lack of horizontal “splat” boundaries and cracks and porosity of ∼22%. The indentation toughness of the SPPS coating was found to be over five times that of the reference 7YSZ APS coating in the most critical in-plane orientation. While the indentation toughness of the SPPS coating is isotropic, the indentation-toughness anisotropy in the APS coating is highly pronounced. Uniaxial compression of the SPPS coatings is characterized by an initial non-linear stress–strain response and permanent deformation. This is followed by a linear-elastic response, before ultimate compressive failure occurs. The ultimate compressive strengths of SPPS and APS coatings in the in-plane orientation were found to be comparable, while the strength of the SPPS coating was found to be lower than that of the APS coating in the out-of-plane orientation. Heat-treatment of the SPPS coating resulted in a significant increase in the ultimate compressive strength in the in-plane orientation, which is most likely due to the complete pyrolysis of the unpyrolyzed material present in the as-sprayed SPPS coatings. The average thermal cycling life of the SPPS TBCs was found to be 820 cycles, while that of a reference APS TBC deposited on identical bond-coated superalloy substrate was found to be 40 cycles. The dramatic improvement in the thermal cycling life in the SPPS TBCs can be attributed to: (i) the significantly higher in-plane local fracture toughness (over five-fold) in the SPPS TBCs over APS TBC and (ii) the presence of the vertical cracks in SPPS TBCs resulting in a high degree of strain tolerance.

Acknowledgements

The authors thank Dr. X. Ma and Mr. J. Roth of Inframat Corporation for providing the precursors and depositing the coatings and Dr. L. Xie for fruitful discussions. This publication was prepared with the support of the US Department of Energy, Office of Fossil Energy, National Energy Technology Laboratory (through a grant from South Carolina Institute for Energy Studies, Grant No. 03-01-SR107). However, any opinions, findings, conclusions or recommendations expressed herein are those of the authors and do not necessarily reflect the views of the DoE.

References

[1] R.L. Jones, in: K.H. Stern (Ed.), Metallurgical and Ceramic Coatings, Chapman & Hall, London, 1996, p. 194.
[2] A.G. Evans, D.R. Mumm, J.W. Hutchinson, G.H. Meier, F.S. Pettit, Prog. Mater. Sci. 46 (2001) 505.
[3] N.P. Padture, M. Gell, E.H. Jordan, Science 296 (2002) 280.
[4] H.E. Eaton, J.R. Linsey, R.B. Dinwiddie, in: T.W. Tong (Ed.), Thermal Conductivity, vol. 22, Technomic, Lancaster, PA, USA, 1994, p. 289.
[5] A. Rabiei, A.G. Evans, Acta Mater. 48 (2000) 3963.
[6] K.W. Schlichting, N.P. Padture, E.H. Jordan, M. Gell, Mater. Sci. Eng. A342 (2003) 120.
[7] J. Karthikeyan, C.C. Berndt, S. Reddy, J.-Y. Wang, A.H. King, H. Herman, J. Am. Ceram. Soc. 81 (1998) 121.
[8] P.R. Strutt, B.H. Kear, R. Boland, U.S. Patent No. 6,025,034 (2000).
[9] N.P. Padture, K.W. Schlichting, T. Bhatia, A. Ozturk, B. Cetegen, E.H. Jordan, M. Gell, S. Jiang, T.D. Xiao, P.R. Strutt, E. Garcia, P. Miranzo, M.I. Osendi, Acta Mater. 49 (2001) 2251.
[10] T. Bhatia, A. Ozturk, L. Xie, E.H. Jordan, B.M. Cetegen, M. Gell, X. Ma, N.P. Padture, J. Mater. Res. 17 (2002) 2363.
[11] L. Xie, X. Ma, E.H. Jordan, N.P. Padture, T.D. Xiao, M. Gell, Mater. Sci. Eng. A362 (2003) 204.
[12] M. Gell, L. Xie, X. Ma, E.H. Jordan, N.P. Padture, Surf. Coat. Technol. 177–178 (2004) 97.
[13] E.H. Jordan, L. Xie, X. Ma, M. Gell, N.P. Padture, B.M. Cetegen, A. Ozturk, J. Roth, T.D. Xiao, P.E.C. Bryant, J. Therm. Spray Technol. 13 (2004) 57.
[14] M.B. Beardsley, in: J. Fairbanks (Ed.), Proceedings of the 1990 Coatings for Advanced Heat Engines Workshop, Department of Energy, Washington, DC, USA, 1990, p. 1153.
[15] S. Suresh, A. Mortensen, Fundamentals of Functionally Graded Materials, IOM Communications Ltd., London, UK, 1998.
[16] B.R. Lawn, Fracture of Brittle Solids, second ed., Cambridge University Press, Cambridge, UK, 1993.
[17] H.D. Steffens, Z. Babiak, M. Gramlich, J. Therm. Spray Technol. 8 (1999) 517.
[18] L. Powlowski, The Science and Engineering of Thermal Spray Coatings, Wiley, New York, NY, 1995.
[19] H. Herman, S. Sampath, R. McCune, MRS Bull. 25 (2000) 17.
[20] L. Xie, X. Ma, A. Ozturk, E.H. Jordan, N.P. Padture, B.M. Cetegen, T.D. Xiao, M. Gell, Surf. Coat. Technol. 183 (2004) 51.
[21] L. Xie, D. Chen, A. Ozturk, F. Wu, X. Ma, E.H. Jordan, B.M. Cetegen, M. Gell, Surf. Coat. Technol., submitted for publication (2005).
[22] E. Wessel, R.W. Steinbrech, Key Eng. Mater. 223 (2002) 55.
[23] A.H. Bartlett, R. Dalmaschio, J. Am. Ceram. Soc. 78 (1995) 1018.
[24] H. Luo, D. Goberman, L.L. Shaw, M. Gell, Mater. Sci. Eng. A346 (2003) 237.
[25] S.R. Choi, D. Zhu, R.A. Miller, Intl. J. Appl. Ceram. Technol. 1 (2004) 330.
[26] E.F. Rejda, D.F. Socie, B.P. Nuel, in: G.R. Halford, J.P. Gallagher (Eds.), Fatigue and Fracture Mechanics, vol. 3, ASTM STP 1389, American Society for Testing of Materials, West Conshohocken, PA, 2000, p. 143.
[27] R.W. Trice, D.W. Prine, K.T. Faber, J. Am. Ceram. Soc. 83 (2000) 3057.
[28] T. Wakui, J. Malzbender, R.W. Steinbrech, J. Therm. Spray Technol. 13 (2004) 390.
[29] C.G. Sammis, M.F. Ashby, Acta Metall. 34 (1986) 511.
[30] B.A. Latella, B.H. O'Connor, N.P. Padture, B.R. Lawn, J. Am. Ceram. Soc. 80 (1997) 1027.
[31] J. Malzbender, R.W. Steinbrech, J. Mater. Res. 18 (2003) 1975.
[32] M. Gell, L. Xie, E.H. Jordan, N.P. Padture, Surf. Coat. Technol. 188–189 (2004) 101.